EEG-27

SENSITIVITY ANALYSIS OF SOLUTE TRANSPORT IN FRACTURES AND DETERMINATION OF ANISOTROPY WITHIN CULEBRA DOLOMITE

Kenneth Rehfeldt

Environmental Evaluation Group
Environmental Improvement Division
Health and Environment Department
P.O. Box 968
Santa Fe, NM 87504

September 1984

STAFF AND CONSULTANTS

James K. Channell, Ph.D., P.E., Environmental Engineer
Lokesh Chaturvedi, Ph.D., Engineering Geologist
Teresa Ortiz, Administrative Secretary
Marshall S. Little([1]), M.S., Health Physicist
Rosella Hinojoza, Secretary
Jack M. Mobley, B.A., Scientific Liaison Officer
Robert H. Neill, M.S., Director
Dan Ramey, M.S., Hydrologist
Kenneth Rehfeldt, M.S., Consulting Hydrologist
Norma I. Silva, Administrative Officer
Donna Shomaker, M.L.S., Librarian
Peter Spiegler([1]) ([2]), Ph.D., Radiological Health Analyst

---

([1]) Certified, American Board of Health Physics
([2]) Certified, American College of Radiology

CONTENTS

LIST OF FIGURES

LIST OF TABLES

1. SENSITIVITY ANALYSIS OF SOLUTE TRANSPORT IN FRACTURES WITHIN THE CULEBRA DOLOMITE

1.1 Introduction

The Waste Isolation Pilot Plant (WIPP) is a U.S. Department of Energy facility for demonstrating the disposal of defense transuranic (TRU) radioactive waste. The WIPP is located approximately 26 miles east of Carlsbad, New Mexico (figure 1). It lies in the northern part of the Delaware Basin, an oval shaped sedimentary trough nearly surrounded by the Capitan reef. The basin is composed primarily of a thick sequence of evaporites with overlying clastic sedimentary rocks. The major formations of interest in the Delaware Basin at the WIPP site consist, in stratigraphially ascending order, the Castile, Salado, and Rustler Formations and the Dewey Lake Redbeds (Figure 2).

The Castile Formation is the basal unit in the evaporite sequence and consists of thick layers of anhydrite and halite. The Castile has been termed anhydrite-rich and is differentiated on this basis from the overlying halite-rich Salado Formation (Lang 1935).

The Salado Formation which overlies the Castile Formation, consists primarily of thick sequences of halite with thin beds of anhydrite, polyhalite, and glauberite. The WIPP repository horizon is located in the lower half of the Salado Formation at a depth of 660 m (2160 ft) below land surface. Beds rich in potassuim minerals such as sylvite, langbeinite and carnallite are locally mined from the McNutt Potash Zone from the middle of the Salado Formation about 200 m (650 ft) above the WIPP horizon and approximately 6 miles north and west of the WIPP. The upper contact of the Salado is a distinct contact between Salado

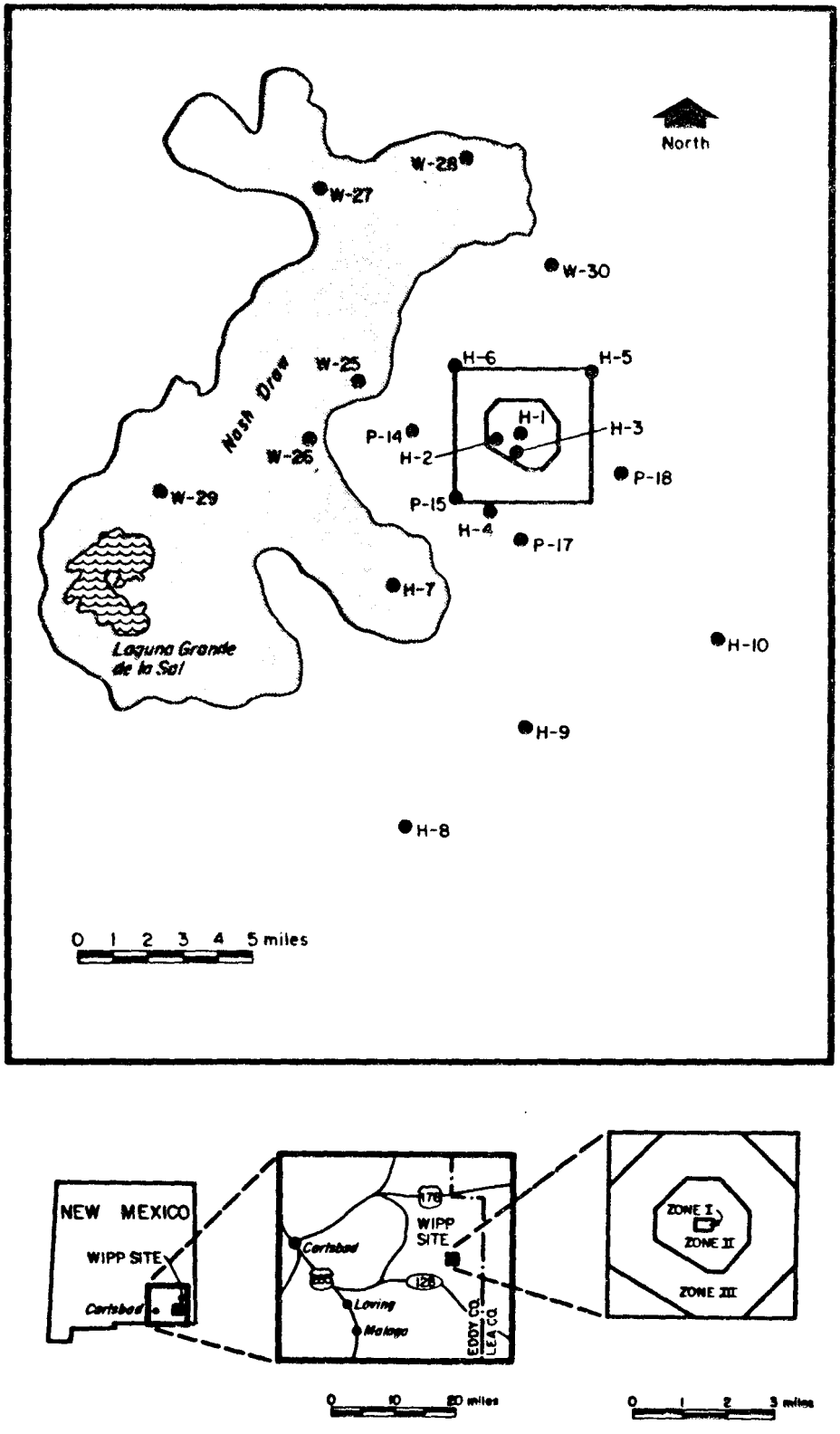

Figure 1. Location of WIPP site.

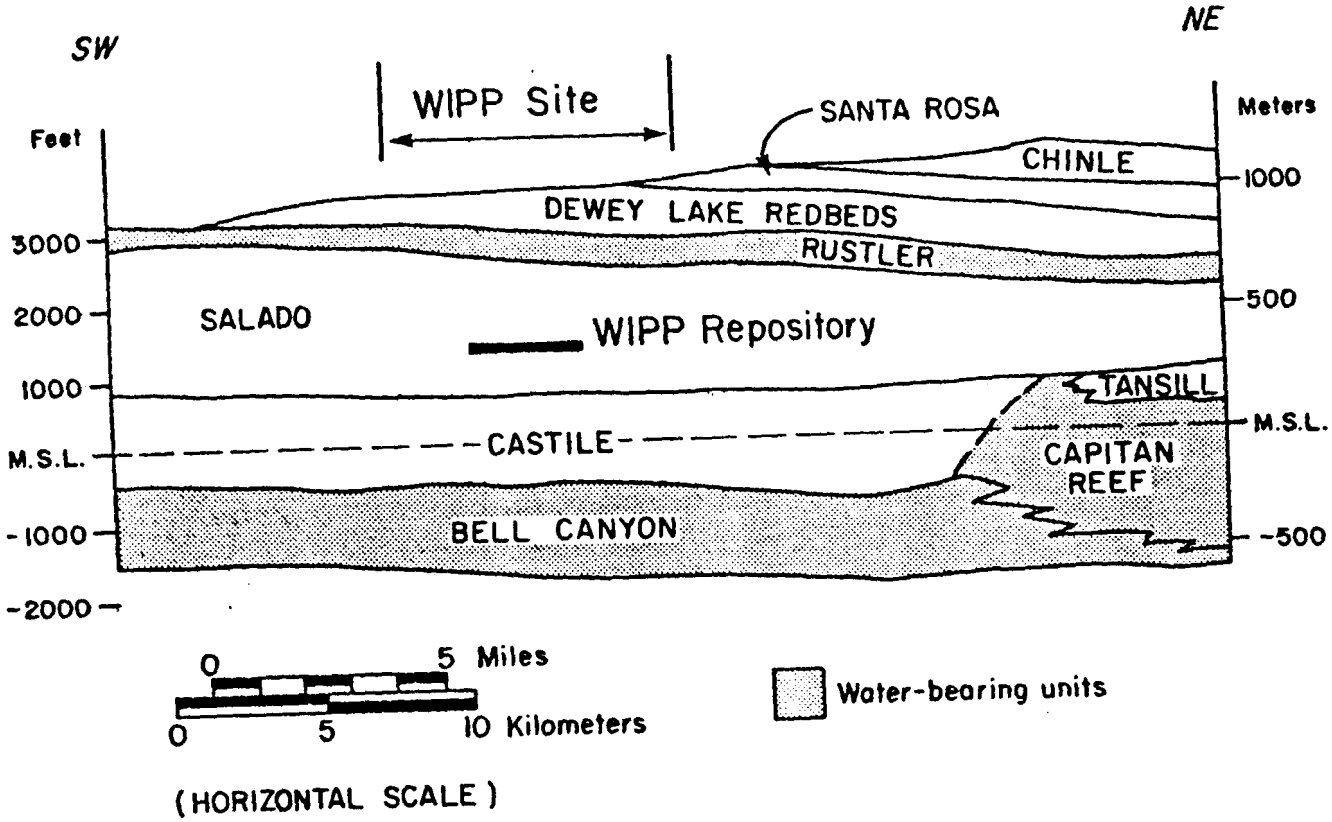

Figure 2. Geologic cross-section at the WIPP Site.

halite and the gray siltstone of the overlying Rustler Formation. A clay layer lies immediately on top of the Salado and has been described as a residue resulting from the dissolution of clay-rich halite at the top of the Salado (Mercer 1983).

The Rustler Formation is the youngest member of the evaporite sequence and is composed primarily of anhydrite with two dolomite beds. The Rustler has been divided into five units which in ascending order are: (1) An unnamed basal clayey siltsone; (2) the Culebra Dolomite, a thin finely-crystalline vuggy dolomite; (3) the Tamarisk Member, an anhydrite with thin layers of clayey silt; (4) the Magenta Dolomite, a thin very finely-grained dolomite; and (5) the Forty-miner member, which is primarily an anhydrite.

Three water bearing zones exist within the Rustler Formation. A minor amount of water is associated with the Rustler/Salado contact at the WIPP site, although this zone is more productive in the western part of the site and in Nash Draw. The Culebra and Magenta Dolomites are the other two water bearing zones within the Rustler Formation. Water flows through these dolomites under confined conditions along bedding planes, fractures, solution conduits, and between interconnected vugs. There are some indications that groundwater may flow through other zones in the Rustler Formation as well. The upper contact of the Rustler Formation is delineated by a lithologic change from anhydrite to siltstone, shale or sandstone of the Dewey Lake Red Beds.

The Dewey Lake Red Beds overlie the Rustler Formation at the WIPP. This sequence of rocks is characterized as alternating beds of reddish-brown siltstones and very-fine-grained sandstones a few inches to several feet thick. The beds are intruded with horizontal and crisscrossed veins of fibrous selenite (gypsum).

Groundwater is the most likely mechanism for transporting radionuclides from the repository to the biosphere. Of the water-bearing units above and below the repository, the Culebra dolomite of the Rustler formation is of most concern. Previous calculations (Wofsy, 1980; Greenfield, 1979; DOE, 1980; Barr et al, 1983) of solute transport within the Culebra are based on the assumption that porous medium flow theory is applicable.

The Culebra is a fractured hydrogeologic unit and consequently the question of whether porous flow theory can simulate the fractured flow is an unanswered question. Barr et al. (1983) have shown that in Nash Draw porous medium theory can be used to reproduce the drawdowns observed in pumping wells. Dugiud et al. (1980) have argued that although porous medium models are often good approximations for flow in fractured media "...transport modeling with the porous medium approach has more problems." This is demonstrated by the unequal arrival time of tracers of the convergent tracer test performed at hydro pad H-6 (Walter, 1983; Gonzalez, 1983).

The H-6 hydro pad consists of three wells forming an equilateral triangle, 100 feet on a side. The wells are labeled H6a, H6b, and H6c; a line connecting H6a and H6c is oriented east-west. Aquifer pumping tests analyzed using porous medium theory (Ward et al., 1983) indicated that the transmissivity is slightly anisotropic with the transmissivity in the H6b-H6c direction about twice that in the H6a-H6c direction. Consequently, all other factors equal, a solute in the H6b-H6c direction should travel about twice as fast as in the H6a-H6c direction. A convergent tracer test (Walter, 1983) was performed by pumping well H6c and simultaneously introducing a slug of different tracers into wells H6a and H6b. The tracers in H6b should have arrived at H6c about twice as fast as the tracers in H6a, but the peak concentration of the H6b tracers arrived 30 times faster and at a concentration 10 times greater than the H6a tracers (Walter, 1983). Flow in the H6b-H6C direction is probably through discrete channels whereas flow in the H6a-H6c direction was through the dolomite matrix or through a very tortuous system of fractures.

Although it would be poor scientific practice to extrapolate the H-6 results to the entire WIPP site because of the proximity of Nash Draw to H-6, the fact that the apparent discrete fracture, or channel, through which the solute traveled was not detected by the aquifer pumping tests is a clear indication that the question of the applicability of fracture flow or porous medium flow theory is very important.

The sophistication of the flow and transport equations for fractured materials greatly exceeds the ability to measure the appropriate parameters in the field. Consequently, many modeling studies of flow in fractured material use porous medium theory for which the parameters are somewhat easier to obtain. At WIPP,

the application of porous medium transport models is not satisfactory because as the H-6 tracer test demonstrates, predictions based on the porous medium theory can lead to significant errors.

One approach to quantifying transport in fractures is to apply simple analytic models which will likely over-estimate the true solute concentration in the medium. Sensitivity analyses of the sample model will indicate the parameters that influence the solute concentration the greatest. Those parameters should be measured in the field to evaluate the significance of fracture flow.

Watt (1983) has shown that radionuclides would travel essentially unretarded from the WIPP to the Pecos River if the groundwater in the Culebra is assumed to flow through discrete, open fractures separated by impermeable blocks of rock. The Culebra dolomite, however, is not an impermeable rock. Therefore, to better treat solute transport in the fractures the diffusion and retardation of solute within the porous matrix must also be considered. The purpose of this section is to investigate the sensitivity of various parameters in an analytic solution of solute transport in a fractured porous medium where the important aspect is the assumption of a porous matrix between fractures.

1.2 Transport Model

Sudicky and Frind (1982) have developed an analytic solution of transient contaminant transport in discrete parallel fractures separated by a porous matrix that accounts for "...advective transport in the fractures, molecular diffusion and mechanical dispersion along the fracture axes, molecular diffusion from the fracture to the porous matrix, adsorption onto the face of the matrix, adsorption within the matrix, and radioactive decay."

They show that the concentration at any point along the fracture is greatest at steady state and therefore only the steady state solution was examined in this work. Additionally, dispersion in the fracture was assumed zero. At steady state this assumption will not create significant error (Sudicky and Frind, 1982).

The steady state solution for the nondispersive case is

$$\frac{c}{c_0} = \exp\left[-\frac{R\lambda Z}{V}(1+\psi)\right] \tag{1}$$

where

$$R = 1 + K_f/b \tag{1a}$$

$$\psi = \frac{\theta(R^1 D^1)^{1/2}}{\lambda^{1/2}\, b\, R}\ \tanh(\sigma\lambda^{1/2}) \tag{1b}$$

$$R^1 = 1 + \rho_b\, K_m/\theta \tag{1c}$$

$$\sigma = (R^1/D^1)^{1/2}(B-b) \tag{1d}$$

$\frac{c}{c_0}$ = relative concentration in the fracture

c_0 = input concentration

λ = radioactive decay constant log e $(2/t_{1/2})$ (T^{-1})

$t_{1/2}$ = half-life of the radionuclide (T)

Z = distance along the fracture (L)

V = flow velocity in the fracture (L/T)

R = fracture face retardation coefficient

R^1 = matrix retardation coefficient

K_f = fracture distribution coefficient (L^3/L^2)

K_m = matrix distribution coefficient (L^3/M)

$2b$ = fracture aperture (L)

$2B$ = distance between fractures (L)

ρ_b = matrix bulk density (M/L^3)

D^1 = matrix diffusion coefficient (L^2/T)

θ = matrix porosity

1.3 Parameter Quantification

The sensitivity analyses were carried out to determine the parameters most important to the concentration of Plutonium-239 in the fracture. For the analyses, a location 10,000 meters from the source was chosen. This distance was chosen to correspond to the maximum distance to the edge of a control zone as defined by NRC. As the WIPP control zone will extend roughly 3,000 meters, the concentrations in this report are less than would be calculated for the WIPP situation. Conversely 10 kilometers is less than the distance from the site to the Pecos River so the concentrations as given here are considered representative.

The parameters of interest for the sensitivity analyses are θ, K_f, K_m, D^1, b, and B. The parameters λ and ρ_b will be fixed at the values below.

$\lambda = 2.83 \times 10^{-5}\ yr^{-1}\ (^{239}Pu)$

$\rho_b = 2.7\ g/cm^3$

The probable ranges of values for the parameters of interest are given below.

$$0.01 \leq \theta \leq 0.20$$

$$1 \times 10^{-8}\ \frac{m^3}{m^2} \leq K_f \leq 10\ \frac{m^3}{m^2} \quad \text{and } K_f = 0$$

$$1 \times 10^{-2}\ \frac{ml}{g} \leq K_m \leq 1 \times 10^{3}\ \frac{ml}{g} \quad \text{and } K_m = 0$$

$$3.2 \times 10^{-4}\ \frac{m^2}{yr} \leq D^1 \leq 3.2 \times 10^{-2}\ \frac{m^2}{yr}$$

$$5 \times 10^{-5}\ m < b < 1 \times 10^{-3}\ m$$

$$4 \times 10^{-2}\ m < B < 50\ m$$

The average velocity in the fracture, V, is obtained from application of the cubic law (Witherspoon, 1980).

$$V = \frac{Q}{A} = \frac{\Delta h}{AL} W \frac{\rho g}{12\mu} (2b)^3$$

where

$\frac{\Delta h}{L}$ = hydraulic gradient; change in head over the distance L

W = height of the fracture

ρ = density of the fluid

g = acceleration of gravity

μ = fluid viscosity

2b = fracture aperture

Q = volumetric flow in a single fracture

A = cross sectional area of the fractue (2b•W)

For subsequent analyses, the parameter values are assigned as

Δh = 250; L = 73,900 feet; W = 23 ft

ρg = 62.4 lb/ft^3; μ = 3.3 x 10^{-5} lb-sec/ft^2

The volumetric flow in a single fracture Q, in ft^3/sec is converted to m^3/year by multiplying by 8.93 x 10^5.

If the total flow (QT) through some cross sectional area of the aquifer is given, then the number of fractures per width of cross-section and the fracture aperture are related by equation 2 and the expression

$$N = \frac{QT}{Q} \qquad (3)$$

where QT - Total flow through the cross sectional area

N - the number of fractures in the cross section

Q - flow in each fracture

To investigate the effect of total flow on the transport equation (1) only the fracture spacing (2B) need be changed, where 2B is the distance between fractures and hence controls the number of fractures (N) per width of cross-section. As mentioned above, the flow through a fractured medium can be often estimated using porous medium theory. Using the transmissivity as measured in H-3, 6935 ft^2/yr, a hydraulic gradient of 0.005, and a width of 1 mile, the flow per mile width is 5,200 m^3/yr-mile. To be conservative, a flow of 6500 m^3/yr-mile is used in subsequent calculations. Table 1 contains the velocity of fluid in a fracture and the spacing for various apertures.

TABLE 1. Velocity of fluid in a fracture and the fracture spacing as a function of fracture aperture assuming a flow of 6,500 m^3/yr-mile.

[2b] Aperture (m)	[V] Average Velocity (m/yr)	[2B] Fracture Spacing (m)
1×10^{-4}	5.5×10^{2}	9.6×10^{-2}
2×10^{-4}	2.2×10^{3}	7.6×10^{-1}
4×10^{-4}	8.8×10^{3}	6.1×10^{0}
6×10^{-4}	2.0×10^{4}	2.1×10^{1}
8×10^{-4}	3.5×10^{4}	4.9×10^{1}
1×10^{-3}	5.5×10^{4}	9.6×10^{1}
1.2×10^{-3}	8.0×10^{4}	1.7×10^{2}
2×10^{-3}	2.2×10^{5}	7.6×10^{2}

1.4 Sensitivity Analyses

The results of the sensitivity analyses are tabulated in Appendix A.

Within the ranges given above, the porosity and matrix diffusion coefficient had very little influence on the concentration in a fracture even for K_m of zero. The fracture face distribution coefficient for the Culebra dolomite is given by Serne et al. (1977) as ranging from 5.9 ml/m^2 to 311 ml/m^2 or 5.9×10^{-6} m^3/m^2 to 3.1×10^{-4} m^3/m^2 for a range of groundwater chemistry from observed groundwater to brine. The sensitivity to K_f was very low for K_f less than 1.0 m^3/m^2. Therefore within the range of observed K_f, the parameter has little effect on the concentration in the fracture.

The remaining parameters are K_m, b and B. The parameter sensitivity is summarized in Figures 3 and 4 which are plots of concentration versus K_m for various fracture apertures (2b). From Figure 3 it is clear that both b and K_m

exhibit a strong influence on the calculated concentration. In general the concentration increases with increasing fracture aperture and decreasing K_m. The influence of the total flow across a cross-section is examined in Figure 4. For fracture apertures (2b) of 2×10^{-4} m or less the effect is significant. For apertures (2b) greater than 4×10^{-4} m no significant effect was noted. The right-hand curve in Figure 4 is the concentration at a point 3,000 meters from the source.

1.5 Discussion of Results

The groundwater travel time in open fractures is very short in comparison to travel time in porous media. Open fractures exist in Nash Draw, at H-6, and are likely present elsewhere at and near the WIPP site. Unfortunately the degree of fracturing, fracture continuity, and the degree of fracture interconnection are unknown. Still it is of importance that the conditions under which fracture flow yields unacceptable concentrations be identified.

Very little retardation of the solute occurs in the fracture. In fact, no significant effect was noted until K_f was nearly 4 orders of magnitude above the measured values (Serne et al., 1977). This result agrees with that of Watt (1983) who assumed flow through fractures separated by impermeable material. One explanation for the minimum retardation in the fractures is the lack of available adsorption sites on the rock surface (Appendix B).

The sensitivity results emphasize the importance of matrix diffusion. Simple diffusion into the rock matrix, however, does not cause a significant reduction in concentration as is evidenced in Figure 3 for small K_m. Therefore, to significantly retard a solute during fracture flow, diffusion into the matrix and retardation in the matrix must occur. To obtain a concentration in a fracture at some level less than the input, an increasing K_m is needed as the fracture aperture increases. It is clear from Figure 3 that truly large, non-conservative K_m's are needed in order to yield c/c_0 less than 1×10^{-3} at a distance of 10 kilometers for fracture apertures (2b) greater than 0.8 mm. Unfortunately, there are few quantitative data regarding fractures in the Culebra. Several Sandia

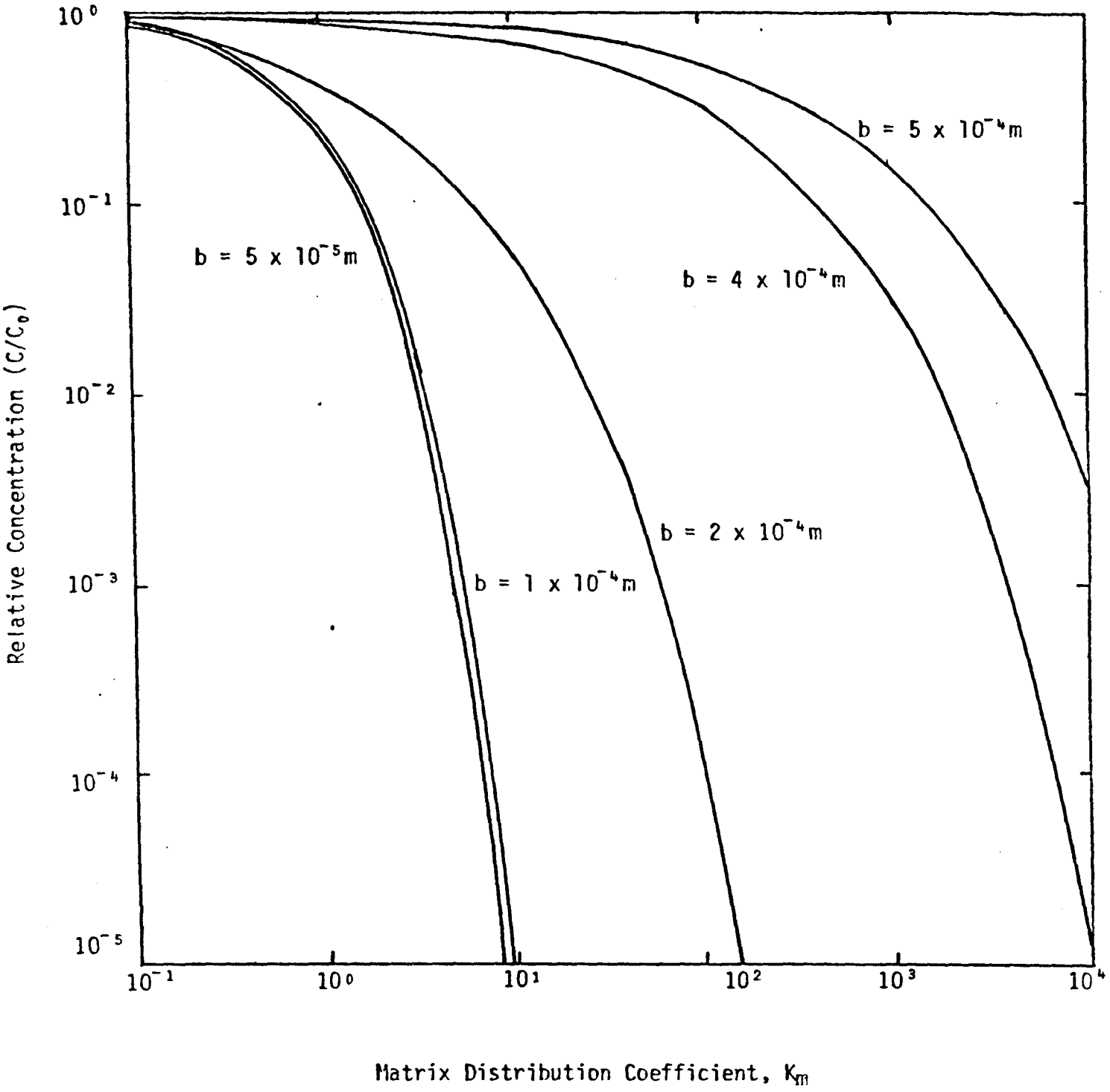

Figure 3. Variation of relative concentration within a fracture at a point 10,000 meters from the source as a function of the matrix distribution coefficient and the fracture aperature.

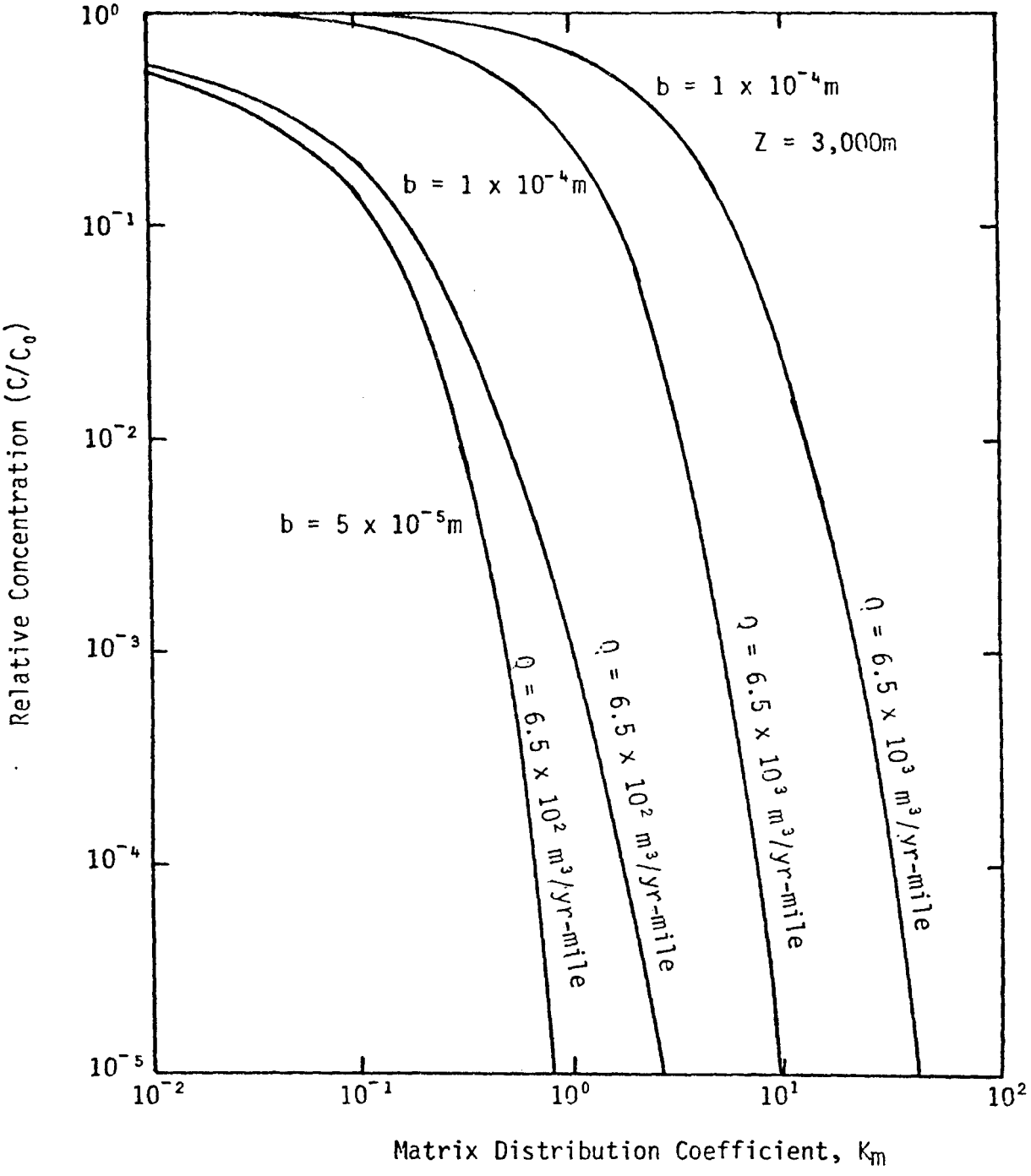

Figure 4. Variation of relative concentration within a fracture at a point 10,000 meters from the source as a function of the matrix distribution coefficient and the total cross-sectional flow.

Laboratory borehole data reports (SAND 79-0276, SAND 79-0280, SAND 79-0283, SAND 79-0284, SAND 81-2643) for boreholes WIPP-19, WIPP-26, WIPP-28, WIPP-30, and WIPP-34, respectively, document fractures in the Culebra, some filled and some open, from hairline to 1 mm wide in aperture. It is unlikely that large (1.0 mm) fractures extend from the site to Nash Draw. However some large, open fractures are known to exist in Nash Draw and travel times in Nash Draw may be more rapid than is predicted from porous medium theory.

From Figure 3 it is clear that if a 0.8 mm fracture, or fractures, exist at the site rapid transport of solute would occur. More likely, small fractures (less than 0.2 mm) exist within the site boundaries and effective retardation is possible for K_m of less than 50 for a distance Z of 3000 m. The most important point to be made is that rapid solute transport with very little solute retardation is possible in fractured flow systems. To date there is very little information concerning fracture aperture, fracture length, degree of fracture filling and the type of fill material. Gibbons and Ferrall (1979) indicate the fractures in the Culebra and Magenta are typically high angle and open, but the amount of filling is highly variable.

Aquifer pumping tests are not likely to yield detailed information on individual fractures because many fracture systems often respond in a manner similar to porous media. Tracer tests are a potential way to characterize the fracture system. However, as evidenced by the H-6 tracer test, the placement of wells can greatly influence a tracer test even if the hydraulics, based on pumping aquifer tests, are similar. Unless two wells intersect a single fracture, or two well connected fractures, the test will not yield reliable information about the transport characteristics of the fracture, or fractures. A tracer test that creates an artificial flow system and forces water to flow through blocks and not along fractures may yield essentially useless data in an aquifer where the flow along fractures dominates the system. Ideally an in situ natural gradient tracer test should be performed. In this test a tracer is introduced into the system and followed as it moves downstream along the natural groundwater flow path. The major drawback to the natural gradient test is the length of time required to have sufficient tracer movement because travel times are less under natural conditions than under induced conditions such as a well. Additionally, at the depth of the Culebra it would be difficult, if not impossible to follow the

tracer. Therefore, it is unrealistic to believe a natural gradient tracer test could be done. As the currently performed tracer tests are of questionable value in characterizing flow in fractures, alternative methods should be employed.

The most sensitive parameters are fracture aperture (2b), and the distribution coefficient of the porous matrix (K_m). Note, however, that K_m is valid only if diffusion into the matrix can be assumed. Measurement of fracture aperture can be made during the sinking of the shafts, from core removed during the drilling of boreholes, or from outcrops. By far the best way would be in the shafts, followed by core or possibly televiewer logs and lastly by outcrop observation. Regional groundwater modeling will yield a reasonable estimate of the total flow, Q. Based on Q, a range of aperture and distance between fractures can be obtained. The range of apertures can then be compared to observed data. Based on the flow presented earlier (6,500 m^3/yr-mile) a reasonable range of apertures would be 0.1 mm to 2mm corresponding to fracture spacings of 5 cm to 380 m, for open, parrallel side fractures. If the fractures are less than ideal, each fracture will carry less water, therefore, more fractures are required to transport a given colume of water and consequently the spacing between fractures is less.

Diffusion into the matrix can be demonstrated by laboratory tests and is a planned part of the WIPP hydrology program (Gonzalez, 1983). The H-6 site may also yield some information about matrix diffusion if additional tests using sorbing tracers are performed. Recall that the sensitivity analysis demonstrated that matrix diffusion alone does not significantly retard the movement of the solute. Sorption of the solute in the matrix must occur before retardation of the solute is significant. Laboratory tests using sorbing tracers flowing through fractures in blocks of Magenta and Culebra Dolomite would help quantify the effect of retardation in the rock matrix. Field tracer tests would provide greater confidence, however, the difficulty of siting the wells to intersect fractures would probably make the field results suspect except at H-6 where there is evidence of a fracture or fractures.

The most immediate work should concentrate on quantifying the fractures; the aperture, the spacing and the amount and type of fracture filling. Quantification of matrix diffusion and solute retardation will then follow.

2. DETERMINATION OF THE ANISOTROPY OF TRANSMISSIVITY IN THE CULEBRA AT THE H-6 AND H-4 HYDROPADS

In order to develop reliable solute transport groundwater models extensive data are required. In addition to storage coefficient, effective porosity, transmissivity, dispersivity, recharge, discharge, leakage, and hydraulic head, the anisotropy of the transmissivity is required. A series of pumping aquifer tests at the H-6 hydropad were used to determine the anisotropy of transmissivity in the Culebra.

Hantush (1966), Hantush and Thomas (1966) Papadopulos (1965), and Ramey (1975) present methods for analyzing pumping aquifer tests in anisotropic media. As presented, these methods required a minimum of 4 wells; one pumping and three observation wells. Recently Walter (1983) has introduced a three well technique for determining anisotropy. Walter applied a regression technique to obtain the anisotropy parameters. A simpler approach utilizing a straight forward application of the procedure given by Papadopulos (1965) is presented below.

2.1 General Theory

The drawdown in a homogeneous, anisotropic confined aquifer resulting from a fully penetrating well producing at a constant rate Q is given by (Papadopulos, 1965)

$$s = \frac{Q}{4\pi \, (T_{xx} \, T_{yy} - T_{xy}^2)^{1/2}} \int_{U_{xy}}^{\infty} \frac{e^{-U_{xy}}}{U_{xy}} \, du \qquad (1)$$

where

$$U_{xy} = \frac{S}{4t} \, \frac{T_{xx} \, y^2 + T_{yy} \, x^2 - 2T_{xy} \, xy}{T_{xx} \, T_{yy} - T_{xy}^2} \qquad (2)$$

s = drawdown (ft)

Q = well discharge (ft^3/day)

t = time after pumping started (days)

x, y = coordinates of observation wells (feet)

S = storage coefficient

T_{xx}, T_{yy}, T_{xy} = components of the second rank symmetric tensor of transmissivity in the x, y coordinate system.

$\int_{U_{xy}}^{\infty} \frac{e^{-U_{xy}}}{U_{xy}} du = W(U_{xy})$ = well function for nonleaky anisotropic confined aquifers.

$(T_{xx}T_{yy} - T_{xy}^2)^{1/2}$ = effective transmissivity, assumed a constant.

Equations 1 and 2 are rearranged as follows

$$Te = \frac{2.3\ Q}{4\pi\ s} \tag{3}$$

$$4t\ U_{xy}\ Te^2 = ST_{xx}\ y^2 + ST_{yy}\ x^2 - 2ST_{xy}\ xy \tag{4}$$

To obtain T_{xx}, T_{yy}, and T_{xy} a pumping aquifer test is performed with drawdowns measured in three observation wells. The data are analyzed by the Theis type-curve method. The coordinates of the match points $W(U_{xy})$ and S are substituted into equation 3 to determine the effective transmissivity $(T_{xx}\ T_{yy} - T_{xy}^2)^{1/2}$. All three observation wells should yield the same value for $(T_{xx}\ T_{yy} - T_{xy}^2)^{1/2}$. The coordinates of each observation well, the match points U_{xy} and t, and the effective transmissivity are substituted into equation 4. The three resulting equations are solved to yield the products ST_{xx}, ST_{yy}, and ST_{xy}. The storage coefficient is determined from

$$S = \frac{ST_{xx}\ ST_{yy} - (ST_{xy})^2}{T_{xx}\ T_{yy} - T_{xy}^2}^{1/2} \tag{5}$$

Finally, T_{xx}, T_{yy}, and T_{xy} are calculated

$$\begin{aligned} T_{xx} &= ST_{xx}/S \\ T_{yy} &= ST_{yy}/S \\ T_{xy} &= ST_{xy}/S \end{aligned} \qquad (6)$$

The Jacob straight-line method can be applied to the observed drawdown data in which case equations 3 and 4 become equations (7) and (8).

$$Te = \frac{2.3\ Q}{4\pi\ \Delta s} \qquad (7)$$

where Δs = the drawdown in one log cycle

and $$2.25\ t_0 Te^2 = ST_{xx}\ y^2 + ST_{yy}\ x^2 - 2\ ST_{xy}\ xy \qquad (8)$$

where t_0 = extrapolation of the straight line to zero drawdown.

The directional transmissivity is given by

$$Tr = r^2 Te^2 S/(ST_{xx}\ y^2 + ST_{yy}\ x^2 - 2S\ T_{xy}\ xy) \qquad (9)$$

The principal components of the transmissivity tensor are given by

$$T_{XX} = 1/2\ \{T_{xx} + T_{yy} + [(T_{xx} - T_{yy})^2 + 4\ T_{xy}^2]^{1/2}\} \qquad (10a)$$

$$T_{YY} = 1/2\ \{T_{xx} + T_{yy} - [(T_{xx} - T_{yy})^2 + 4\ T_{xy}^2]^{1/2}\} \qquad (10b)$$

where X and Y are the coordinate axes of the principal components of the Transmissivity tender.

The angle between the x and X axes, positive in a counterclockwise direction is

$$\theta = \arctan \frac{T_{XX} - T_{xx}}{T_{xy}} \qquad (10c)$$

2.2 Three Well Technique

As presented above, four wells are required in order to determine T_{XX}, T_{YY} and 0. Walter (1983) has demonstrated that only three wells are needed. Following the convention of Walter, a working coordinate system x_i, y_i is defined at each well (Figure 5). When Well B is pumped, the observed drawdowns at wells C and A are input into equations 3 and 4, or 7 and 8. Two of the three equations needed to solve for ST_{xx}, ST_{yy}, and ST_{xy} are

$$2.25\ t_0{}^C\ Te^2 = ST_{xx}\ (y_B{}^C)^2 + ST_{yy}(x_B{}^C)^2 - 2\ ST_{xy}\ x_B{}^C\ y_B{}^C \qquad (11\ a)$$

and

$$2.25\ t_0{}^A\ Te^2 = ST_{xx}(y_B{}^A)^2 + ST_{yy}\ (x_B{}^A)^2 - 2\ ST_{xy}\ x_B{}^A\ (y_B{}^A) \qquad (11\ b)$$

where the notation $X_B{}^A$ represents the x-coordinate of observation well A relative to pumping well B.

By pumping well C and observing the drawdowns in wells A and B two more equations can be written

$$2.25\ t_0{}^A\ Te^2 = ST_{xx}(y_C{}^A)^2 + ST_{yy}(x_C{}^A)^2 - 2\ ST_{xy}\ x_C{}^A y_C{}^A \qquad (11\ c)$$

and

$$2.25\ t_0{}^V Te^2 = ST_{xx}\ (y_C{}^B)^2 + ST_{yy}\ (x_C{}^B)^2 - 2ST_{xy}\ x_C{}^B\ y_C{}^B \qquad (11\ d)$$

Equations 11a and 11d are not linearly independent, therefore only 2 sets of equations can be solved 11a, 11b, 11c, and 11b, 11c, 11d. Theoretically these two sets should yield the same result. However, data uncertainties coupled with measurement inaccuracies will likely yield two different, but hopefully similar results.

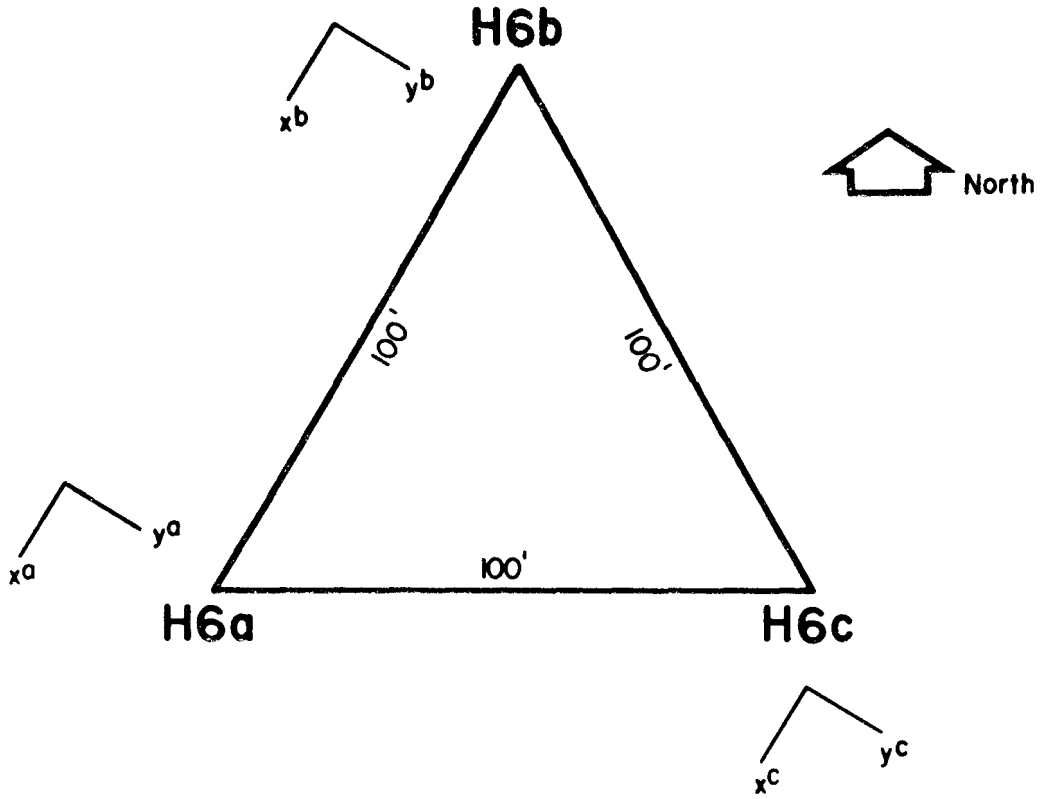

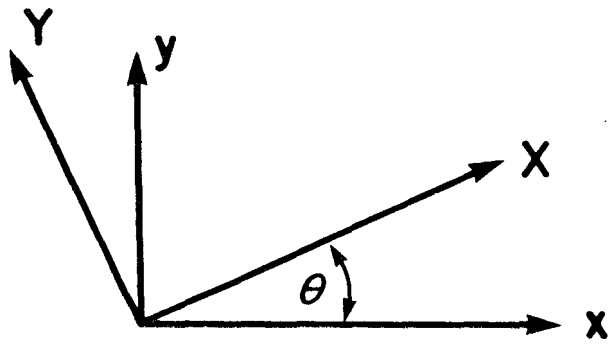

X-Y Principal coordinates of the anisotropy tensor

x-y Working coordinates

Figure 5. H-6 hydropad and coordinate system.

If well A is also pumped, then 2 more equations are available

$$2.25\ t_0{}^B\ Te^2 = ST_{xx}(y_A{}^B)^2 + ST_{yy}(x_A{}^B)^2 - 2\ ST_{xy}\ x_B{}^C\ y_A{}^B \qquad (11$$

$$e)2.25\ t_0{}^C\ Te^2 = ST_{xx}(y_C{}^A)^2 + ST_{yy}(x_A{}^C)^2 - 2\ ST_{xy}\ x_A{}^C\ y_A{}^C \qquad (11\ f)$$

Equations 11b and 11e and equations 11c and 11f are not linearly independent. Combining of equations (11) yields 8 groups of linearly independent equations.

1) 11a, 11b, and 11c
2) 11a, 11c, and 11e
3) 11a, 11e, and 11f
4) 11a, 11b, and 11f
5) 11b, 11c, and 11d
6) 11b, 11d, and 11f
7) 11d, 11e, and 11f
8) 11c, 11d, and 11e (12)

The solution of each set of equations in (12) and equations (6) and (10) will yield an estimate of T_{xx}, T_{yy}, and θ. If well A is pumped twice, at two different rates, then 4 equations 11a, $11a^1$, 11b, $11b^1$, where the prime represents the second pumping rate, are obtained. The primed equations from pumping A can be combined with the unprimed equations of pumping A, B, and C, to yield a total of 18 sets of linearly independent equations.

2.3 Application

Detailed hydrogeologic studies at the Waste Isolation Pilot Plant Site, Southeastern New Mexico, began in 1977 and are ongoing. The majority of the studies have concentrated on the Culebra Dolomite unit of the Rustler Formation which lies roughly 450 meters above the proposed repository. The groundwater hydrology of the WIPP site is described by Mercer and Orr (1979), Gonzalez (1983) and Mercer (1983). The H-6 hydropad is located northwest of the proposed

repository (Figure 1). The three wells form an equilateral triangle (Figure 5) 100 feet on a side. The well construction, pumping data and drawdown data are given by Ward and others (1983). For subsequent analyses the Jacob semilog method is used. From equation 7 it is clear that in order for Te to be equal at each observation well the slope of the data must be the same on the semilog plot, for equal pumping, Q. With the three well technique, however, two wells must be pumped to get three independent equations and it is unlikely that the same pumping rate will be attained in both wells. Therefore, with the three-well technique and the standard Jacob-semilog plot the drawdown data from 2 observations wells may have different slopes yet yield similar Te because of differences in the rate of pumping. This makes the analysis slightly more difficult than in the case where only a single well is pumped.

To simplify the analyses a modified Jacob semilog plot of normalized drawdown (s/Q) versus log t is used. In this manner the different pumping rates at the two wells are accounted for and therefore the slope of each data curve should be the same.

The H-6 hydropad configuration is given in Figure 5. The working coordinate system was chosen such that the x-axis was in the direction of the well pair H6a-H6b. During testing well H6b was pumped once and H6c was pumped twice. The three pumping tests are called test 1, test 2, and test 3 corresponding to pumping H6b, the first H6c pumping, and the second H6c pumping, respectively. Referring to equations (11), six equations can be written 11a, 11b, 11c, 11d, $11c^1$, $11d^1$ where the primed equations indicate the second pumping of well H6c. From these six equations, six linearly independent sets of equations can be solved:

1) 11a 11b 11c
2) 11b 11c 11d
3) 11a 11b $11c^1$
4) 11b $11c^1$ $11d^1$
5) 11b 11c $11d^1$
6) 11b $11c^1$ 11d

The plots of normalized drawdown versus log time are presented in Figure (6) for tests 1, 2, and 3. Table 1 summarizes the data used in solving equations 7, 8, 9, and 10 and Table 2 contains the resulting parameters which are graphically displayed in Figure 3. Table 3 contains the directional transmissivity at each well for each set of equations.

2.4 Discussion of Results at H-6

The results presented in Figure 3 show some scatter, yet with the possible exception of equation set 6, the results are fairly consistent. Still it is difficult to ascertain the directions of the anisotropy tensor due to the variation in θ. The ambiguity is significantly reduced, however, if the square root of the principal components of the transmissivity tensor ($\sqrt{T_{xx}}$, $\sqrt{T_{yy}}$) are plotted as single data points as in Figure 8. The data form an ellipse which can be viewed as an average, or mean of the results from the six sets of equations. The directional transmissivities (Tr) also shown on Figure 8, correspond extremely well with the mean ellipse. Therefore, the mean ellipse, based on all the available data, is deemed an accurate representation of the anisotropy of the transmissivity at the H-6 hydropad. The parameters derived from the mean ellipse are:

$$T_{XX} = 125 \text{ ft}^2/\text{day}$$
$$T_{YY} = 44 \text{ ft}^2/\text{day}$$
$$T_{XX}/T_{YY} = 2.9$$
$$\theta = 30°$$

These results demonstrate that the direction of the major component of the transmissivity tensor may be oriented north-south. Clearly, from the results in Table 3, other anisotropy parameters would be obtained if only a portion of the data were selectively used. Therefore, it is important to view published anisotropy parameters as estimates and that the true values may differ from those estimates.

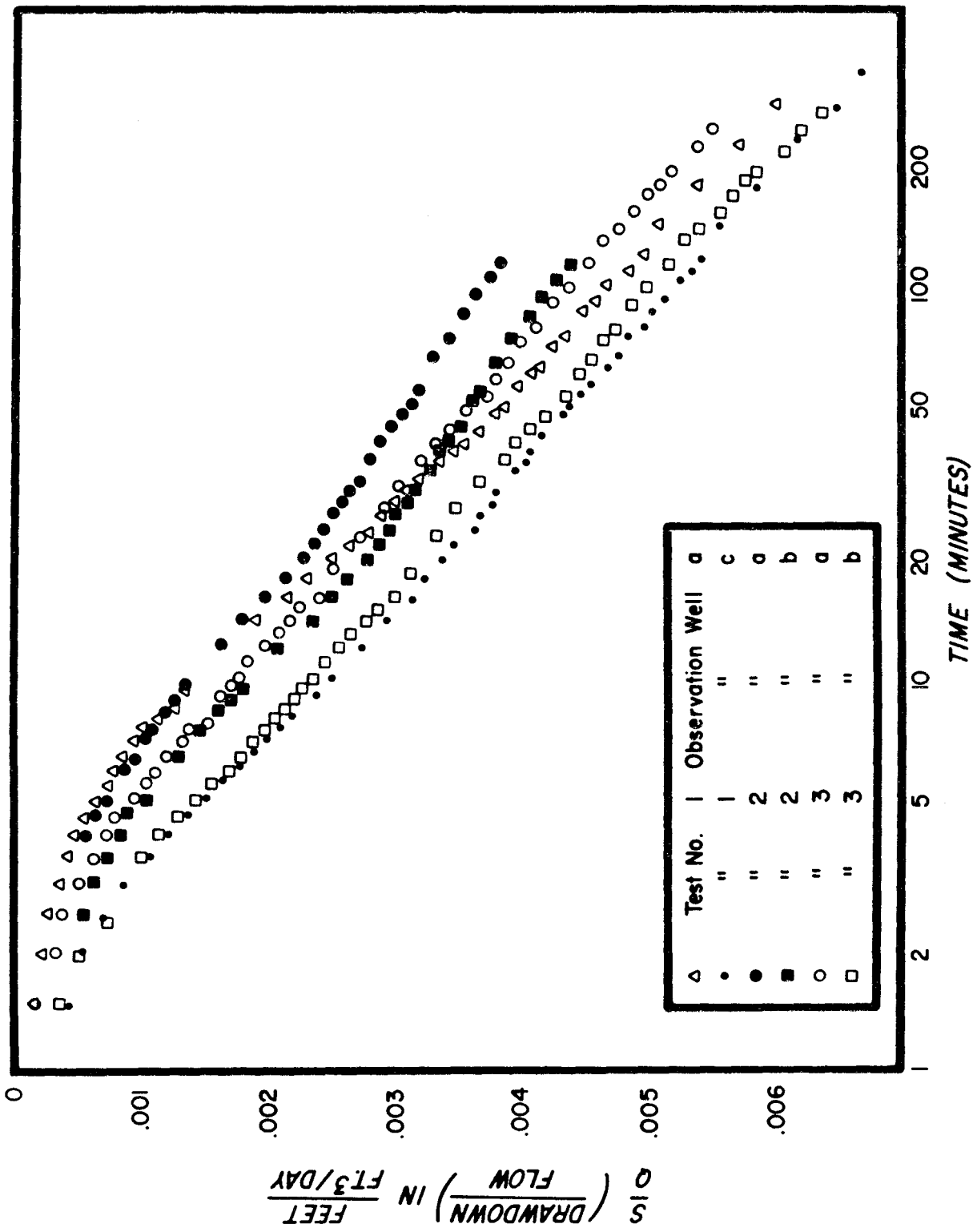

Figure 6. Semi-log plot of normalized drawdown for all pumping tests at hydropad H-6.

Table 2. H-6 Parameters Needed to Solve for Anisotropy

Equation Set	Slope	Te	Equation Number	t_0 (min)	2.25 t_0(days)Te^2	x (ft)	y (ft
1	.0027	68.0	11a	1.14	8.25	50	86.6
			11b	1.80	13.02	100	0
			11c	3.88	28.07	50	-86.6
2	.0024	75.6	11b	1.16	10.37	100	0
			11c	2.75	24.58	50	-86.6
			11d	1.67	14.93	-50	-86.6
3	.0026	69.6	11a	1.03	7.79	100	0
			11b	1.70	12.86	50	86.6
			11c[1]	2.10	15.89	50	-86.6
4	.0026	69.9	11b	1.62	12.35	100	0
			11c[1]	2.10	16.01	50	-86.6
			11d[1]	1.19	9.07	-50	-86.6
5	.0025	72.1	11b	1.48	12.01	100	0
			11c	2.05	16.63	50	-86.6
			11d[1]	1.03	8.36	-50	-86.6
6	.0025	74.1	11b	1.42	12.18	100	0
			11c[1]	1.80	15.44	50	-86.6
			11d	1.90	16.30	-50	-86.6

Table 3. H-6 Anisotropy Results

Equation Set	Transmissivity $T_{XX}(ft^2/day)$	$T_{yy}(ft^2/day)$	$\frac{T_{XX}}{T_{YY}}$	Angle θ (°)	Storage Coef. S
1	171	27	6.3	37	1.66×10^{-5}
2	132	44	3.0	21	1.90×10^{-5}
3	105	46	2.3	49	1.61×10^{-5}
4	98	50	2.0	44	1.69×10^{-5}
5	109	48	2.3	43	1.58×10^{-5}
6	88	62	1.4	-7	1.95×10^{-5}
Mean	117	46	2.9	31	1.73×10^{-5}
St. dev.	30	11	1.8	21	$.15 \times 10^{-5}$

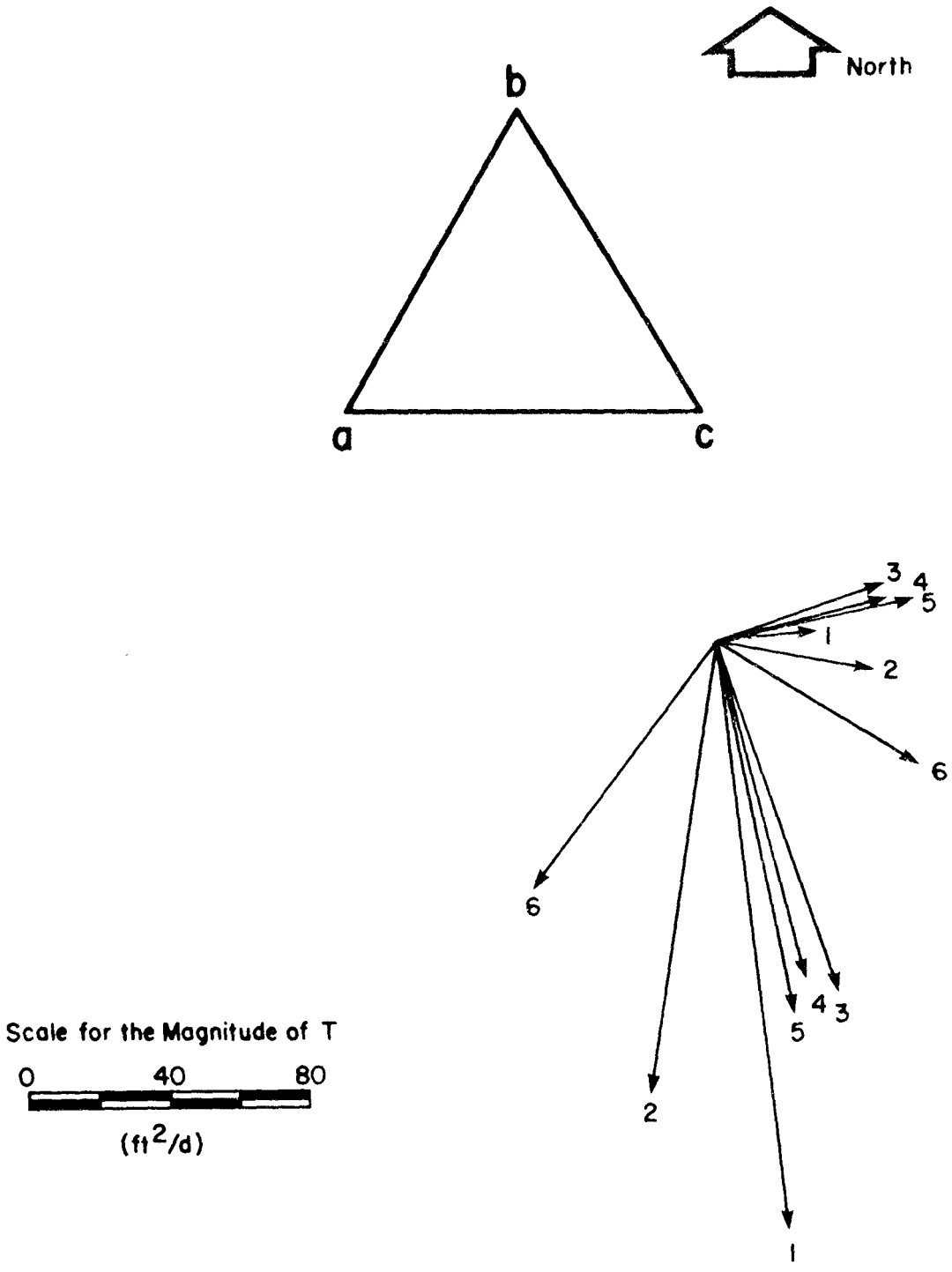

Figure 7. Magnitude and direction of the principal coordinates of the transmissivity tensor at the H-6 hydropad for equation sets 1 through 6.

Table 4. H-6 Directional Transmissivity

Equation Set	Pumped Well	Observation Well	Directional Transmissivity (feet^2/day)
1	b	a	59.0
	b	c	93.0
	c	a	27.4
2	b	a	105.0
	c	a	44.3
	c	b	72.7
3	b	c	100.0
	b	a	60.6
	c	a	49.1
4	b	a	66.8
	c	a	51.6
	c	b	91.0
5	b	a	68.4
	c	a	49.5
	c	b	98.3
6	b	a	87.9
	c	a	69.3
	c	b	65.7

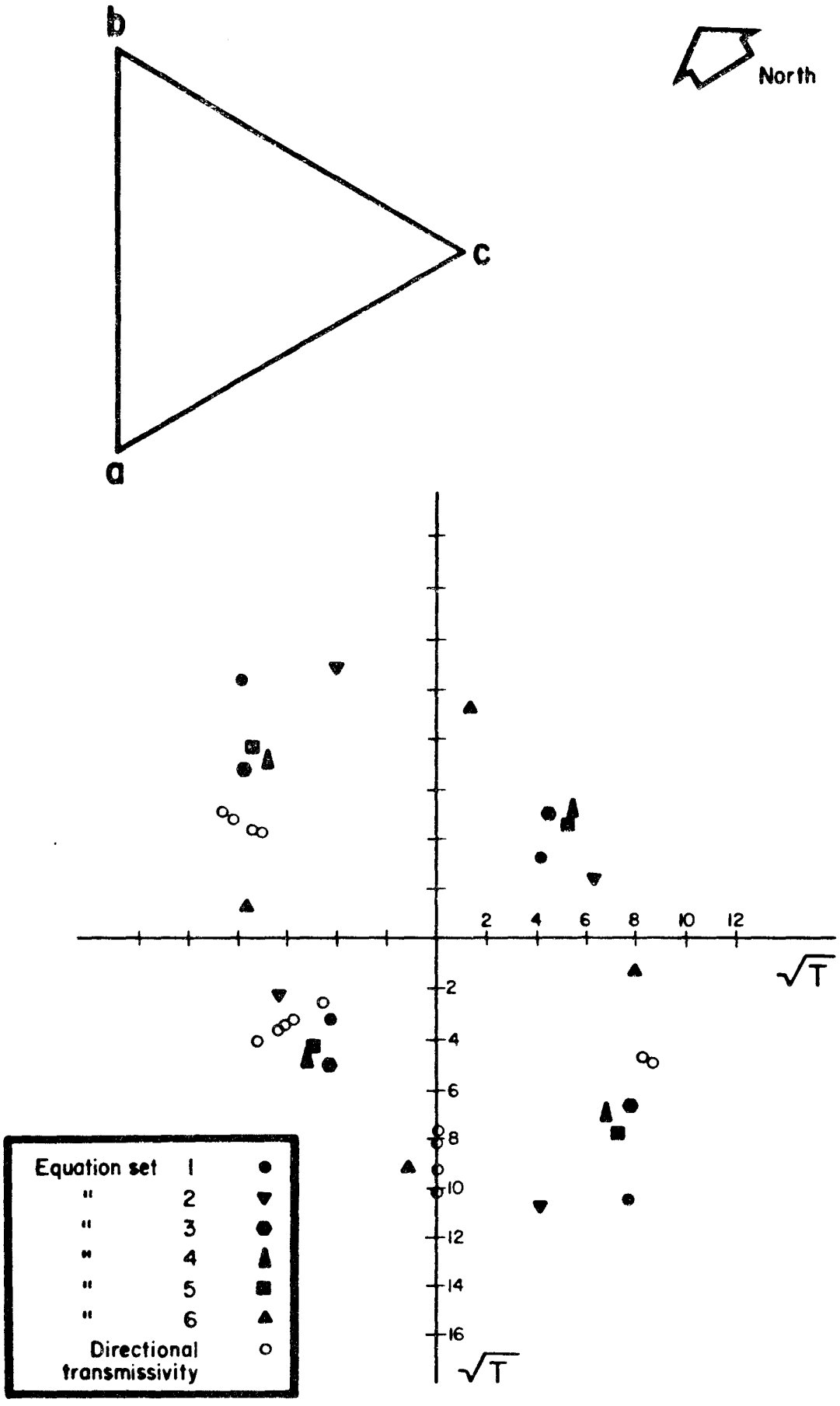

Figure 8. Transmissivity ellipse for the H-6 hydropad.

2.5 Discussion of Results at H-4 Hydropad

The H-4 hydropad configuration is given in Figure 9. The working coordinate system was chosen such that the x-axis parallels the H4b - H4c direction. The pumping schedule was the same as for H-6, therefore six sets of equations can be solved. The normalized drawdown versus log time is given in Figure 10. The data used to solve equations 7, 8, 9, and 10 and the resulting parameters are presented in Tables 5 and 6, respectively. The results of Table 6 are graphically displayed in Figure 11. Note that the transmissivities from equation sets 4 and 5 have been corrected to a Te of 0.85 on Figure 11. Table 7 contains the directional transmissivities.

As was the case with the H-6 tests, the mean H-4 anisotropy ellipse (Figure 11) has a consistent pattern. The direction of the major principal component of the anisotropy tensor is oriented about 20° west of south, or roughly south-southwest. These results are consistent with those of H-6 and indicate an underlying transmissivity tensor, the major component of which lies north-south or possibly southwest-northeast.

Again as with H-6, a careful selection of data would produce results other than the mean parameters derived here. At both H-4 and H-6 one or two equation sets appear to be best suited for analyses based on visual inspection of the normalized drawdown - log time curves. However, to selectively choose those equation sets amounts to little more than choosing the data to fit the theory. It is my feeling that by using all the data, a better estimate of the true anisotropy is obtained.

2.6 Conclusions of Anisotropy

The technique of analyzing the pumping test data from a 3 well hydropad for anisotropy of transmissivity presented above is relatively straight-forward and easily performed using a desk-top calculator. The significant result of this study is that the major principal axes of the anisotropy tensor appears to be oriented north-south or southwest-northeast rather than northwest-southeast as has been presented by Gonzalez (1983). This reorientation of the transmissivity could influence the model results of Barr et al. (1983). Therefore, the sensitivity of the model to varied anisotropy parameters should be documented.

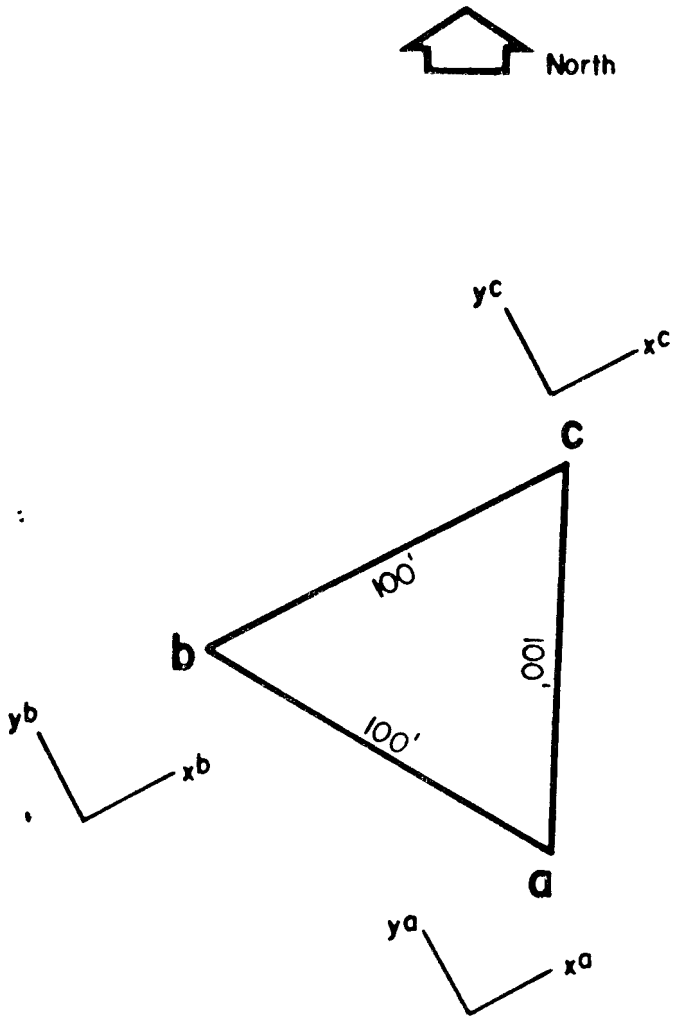

Figure 9. Orientation of the H-4 hydropad.

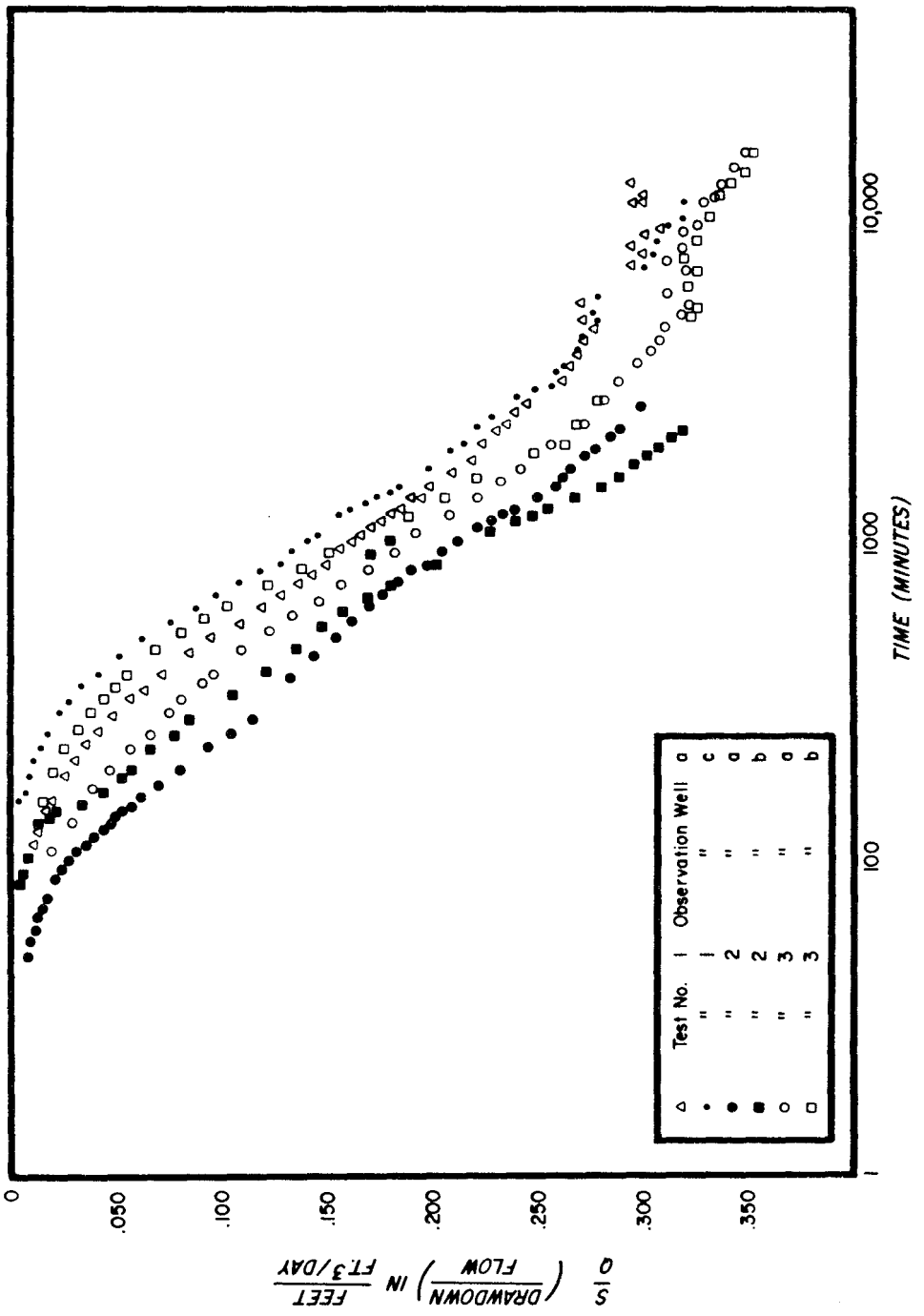

Figure 10. Semi-log plot of normalized drawdown for all pumping tests at hydropad H-4.

Table 5. H-4 Parameters Used to Solve for Anisotropy

Equation Set	Slope	Te	Equation Number	t_0 (min)	2.25 t_0(days)Te^2	x (ft)	y (ft)
1	.221	.83	11b	172	.184	50	-86.6
			11a	212	.227	100	0
			11c	104	.111	-50	-86.6
2	.213	.86	11b	160	.184	50	-86.6
			11c	91	.105	-50	-86.6
			11d	66	.076	-100	0
3	.223	.82	11b	177	.186	50	-86.6
			11a	210	.221	100	0
			11c[1]	133	.140	-50	-86.6
4	.165	1.11	11b	84	.161	50	-86.6
			11c[1]	54	.103	-50	-86.6
			11d[1]	52	.100	-100	0
5	.167	1.10	11b	86	.161	50	-86.6
			11c	41	.077	-50	-86.6
			11d[1]	56	.105	-100	0
6	.220	.83	11b	172	.186	50	-86.6
			11d	74	.080	-100	0
			11c[1]	130	.141	-50	-86.6

Table 6. H-4 Anisotropy Results

Equation Set	TXX	TYY	$\frac{T_{XX}}{YY}$	θ (°)	S
1	1.249	.549	2.3	71	1.94×10^{-5}
2	1.551	.476	3.3	23	1.20×10^{-5}
3	1.068	.631	1.7	73	2.15×10^{-5}
4	1.557	.789	2.0	29	1.04×10^{-5}
5	1.74	.69	2.5	40	9.42×10^{-6}
6	1.355	.511	1.8	13	1.45×10^{-5}
Mean	1.42	.61	2.3	42	1.45×10^{-5}
St. dev.	.24	.12	.6	25	$.49 \times 10^{-5}$

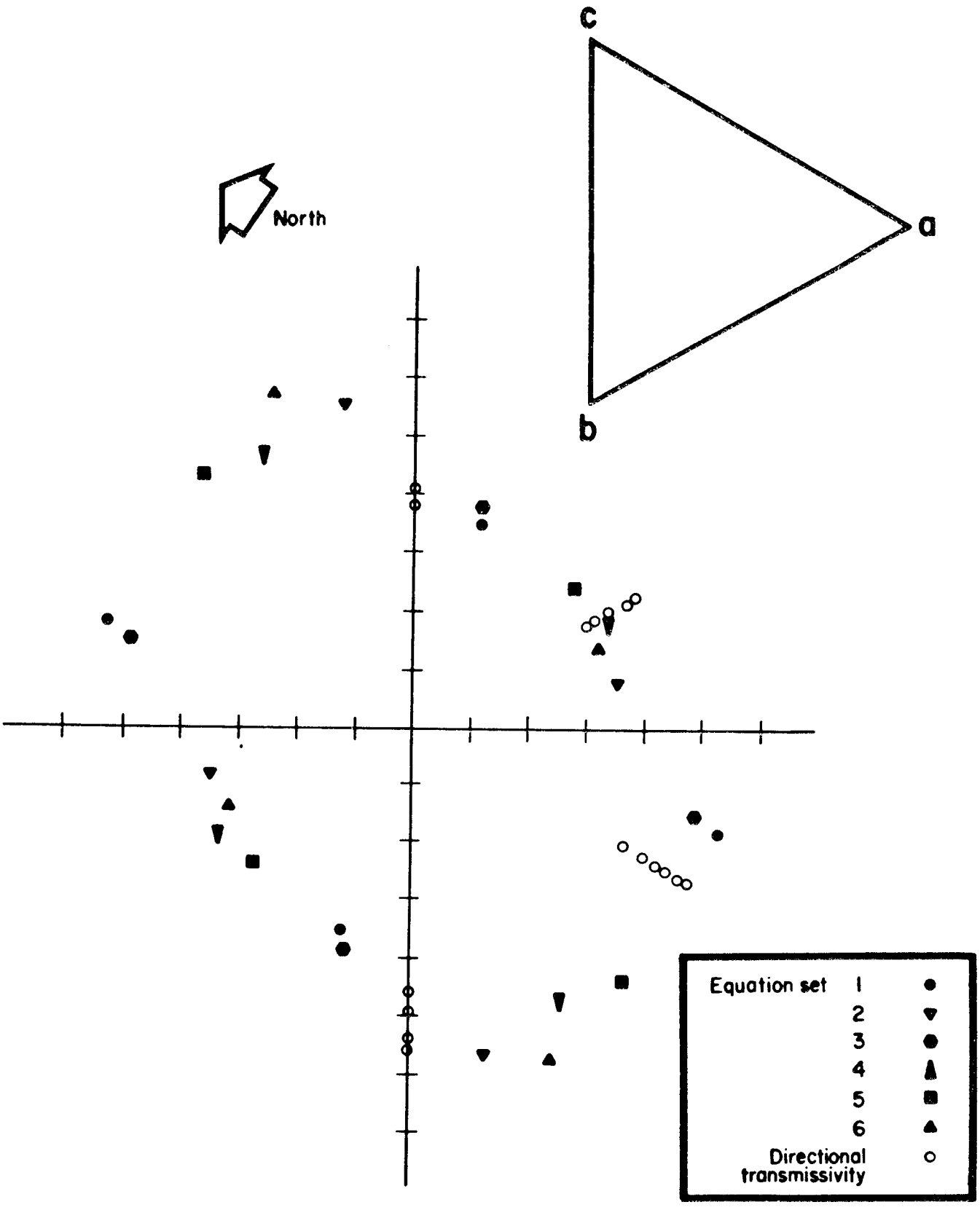
c
a
b
North
Equation set 1
2
3
4
5
6
Directional transmissivity

Table 7. H-4 Directional Transmissivity

Equation Set	Pumped Well	Observation Well	Directional Transmissivity (feet^2/day)
	b	a	.73
1	b	c	.59
	c	a	1.20
	b	a	.48
2	c	a	.85
	c	b	1.17
	b	a	.78
3	b	c	.65
	c	a	1.03
	b	a	.80 (.66)[1]
4	c	a	1.26 (.96)[1]
	c	b	1.29 (.99)[1]
	b	a	.71 (.55)[1]
5	c	a	1.48 (1.14)[1]
	c	b	1.09 (.84)[1]
	b	a	.54
6	c	b	1.25
	c	a	.71

[1]Data in parenthesis correspond to a Te of 0.85 ft^2/day.

3. References Cited

Barr, G. E., W. B. Miller, and D. D. Gonzalez, 1983, Interim Report on the Modeling of the Regional Hydraulics of the Rustler Formation: Sandia National Laboratories, Report SAND 83-0391.

Department of Energy, 1980, Final Environmental Impact Statement -- Waste Isolation Pilot Plant: United States Department of Energy, 2 volumes.

Duguid, I. O. and others, 1980, Panel Discussion: in Wang, J. S. Y., ed., Proceedings of a Workshop on Numerical Modeling of Thermohydrological Flow in Fractured Rock Masses, Lawrence Berkley Laboratory, Report LBL-11566, 125 p.

Gibbons, J. F., and C. C. Ferrall, 1980, Fracture Model of Rustler Formation at the WIPP Site: unpublished CSI report.

Gonzales, D. D., 1983, Groundwater Flow in the Rustler Formation, Waste Isolation Pilot Plant (WIPP), southeast New Mexico (SEM): Interim Report: Sandia National Laboratories, Report SAND 82-1012, 39 p.

Greenfield, M. A., 1979, Simple Model for Estimating Maximum Radionuclide Concentrations in the Pecos River, and Associated Ingestion Doses, Due to the Release of Radioactivity from the WIPP Repository: Appendix VI in Neill, R. H., J. K. Channell, C. Wofsy, and M. A. Greenfield, eds., Radiological Health Review of the Draft Environmental Impact Statement (DOE/EIS-0026-D) Waste Isolation Pilot Plant, U. S. Department of Energy, Environmental Evaluation Group, Report EEG-3.

Hantush, M. S., 1966, Analysis of Data from Pumping Tests in Anisotropic Aquifers: Journal of Geophysical Research, vol. 71, no. 2, p. 421-426.

Hantush, M. S., and R. G. Thomas, 1966, A Method for Analyzing a Drawdown Test in Anisotropic Aquifers: Water Resources Research, vol. 2, no. 2, p. 281-285.

Mercer, J. W. and B. O. Orr, 1979, Interim Data Report on the Geohydrology of the Proposed Waste Isolation Pilot Plant Site, Southeast New Mexico: U. S. Geological Survey Water-Resources Investigations Report 79-98, 178 p.

Papadopulos, I. S., 1965, Nonsteady Flow to a well in an Infinite Anisotropic Aquifer: International Association of Scientific Hydrology, Symposium of Dubrovnik, vol. 1, p. 21-31.

Ramey H. J. Jr.,1 1975, Interference Analysis for Anistropic Formations - A Case History: Journal of Petroleum Technology, p. 1290 -1298.

Sandia, 1979, Basic Data Report for Drillhole WIPP-26 (Waste Isolation Pilot Plant-WIPP): Sandia National Laboratories, Report SAND 79-0280.

Sandia, 1979, Basic Data Report for Drillhole WIPP-29 (Waste Isolation Pilot Plant-WIPP): Sandia National Laboratories, Report SAND 79-0283.

Sandia, 1980, Basic Data Report for Drillhole WIPP-19 (Waste Isolation Pilot Plant-WIPP): Sandia National Laboratories, Report SAND 79-0276.

Sandia, 1980, Basic Data Report for Drillhole WIPP-30 (Wste Isolation Pilot Plant-WIPP): Sandia National Laboratories, Report SAND 79-0284.

Sandia, 1981, Basic Data Report for Drillhole WIPP-34 (Waste Isolation Pilot Plant-WIPP): Sandia National Laboratories, Report SAND 81-2643.

Serne, R. J., D. Rai, M. J. Mason, and M. A. Molecke, 1977, Batch K_d Measurements of Nuclides to Estimate Migration Potential at the Proposed Waste Isolation Pilot Plant in New Mexico: Battelle Pacific Northwest Laboratories, Report PNL-2448, 81 p.

Sudicky, E. A. and E. O. Frind, 1982, Contaminant Transport in Fractured Porous Media: Analytical Solutions for a System of Parallel Fractures: Water Resources Research, Vol. 18, no. 6, p. 1634-1642.

Walter, G. B., 1983, Convergent Flow Tracer Test at H-6: Waste Isolation Pilot Plant (WIPP) Southeast New Mexico: Sandia National Laboratories, Report SAND 83-7015.

Ward, J. J., G. B. Walter, and D. D. Gonzalez, 1983, Aquifer Tests to Determine the Principal Components of Transmissivity in the Culebra Dolomite at Hydropods H-4, H-5, and H-6: Waste Isolation Pilot Plant (WIPP), Southeast New Mexico: Sandia National Laboratories, Report SAND 83-7009.

Watt, R. E., 1983, Letter of June 16, 1983, to the Governor of New Mexico, Toney Anaya.

Witherspoon, P.A., J.S.Y. Wang, K. Iwai and J.E. Gale, 1980, Validity of Cubic Law for Fluid Flow in a Deformable Rock Fracture. Water Resources Research, 16(6), 1016 - 1024.

Wofsy, Carla, 1980, The Significance of Certain Rustler Aquifer Parameters for Predicting Long-Term Radiation Doses from WIPP: Environmental Evaluation Group, Report EEG-8.

APPENDIX A

APPENDIX A

Numerical Results of Sensitivity Analyses

A1) Porosity (θ)

θ	$K_m = 0$ $\frac{c}{c_0}$	$K_m = 0.1$ $\frac{c}{c_0}$	$K_m = 1.0$ $\frac{c}{c_0}$
0.01	.995	.981	.289
0.05	.974	.961	.251
0.10	.950	.936	.240
0.15	.925	.913	.233
0.20	.902	.889	.226

$K_f = 0.0$; $D^1 = 3.15 \times 10^{-3}$ m/yr

$b = 1 \times 10^{-4}$ m; B = 0.4 m

A2) Fracture Distribution Coefficient (K_f)

K_f	$K_m = 0.0$ $\frac{c}{c_0}$	$K_m = 1.0$ $\frac{c}{c_0}$
1×10^{-8}	.950	.240
1×10^{-3}	.948	.240
1×10^{-1}	.835	.211
1×10^{0}	.261	6.6×10^{-2}
1×10^{1}	2.3×10^{-6}	5.9×10^{-7}

$D^1 = 3.15 \times 10^{-3}$ m/yr; $b = 1 \times 10^{-4}$m; B = 0.4 m

A3) Diffusion Coefficient (D^1)

D^1	$K_m = 0.01$ $\frac{c}{c_0}$	$K_m = 1.0$ $\frac{c}{c_0}$
3.15×10^{-4}	.937	.279
3.15×10^{-3}	.936	.240
3.15×10^{-2}	.936	.236

$\theta = 0.1$; Kf = 0.0; $b = 1 \times 10^{-4}$; B = 0.4; $D^1 = 3.15 \times 10^{-3}$ m/yr.

A4) Flow - variation of B

b	B_1	$\frac{c}{c_{0\ 1}}$	$B_2 = 10B_1$	$\frac{c}{c_{0\ 2}}$
5×10^{-5}	0.05	.949	.5	.520
1×10^{-4}	.4	.950	4	.611
2×10^{-4}	3.0	.954	30	.845
5×10^{-4}	48	.989	480	.989

$K_m = 0.0$; $K_f = 0.0$; $\theta = 0.1$; $D^1 = 3.15 \times 10^{-3}$ m/yr.

b	B_1	$\frac{c}{c_{0\ 1}}$	$B_2 = 10B_1$	$\frac{c}{c_{0\ 2}}$
5×10^{-5}	0.05	8.9×10^{-7}	.5	1.8×10^{-51}
1×10^{-4}	.4	4.1×10^{-6}	4	1.9×10^{-10}
2×10^{-4}	3	6.1×10^{-2}	30	6.1×10^{-2}
5×10^{-4}	48	.836	480	.836

Km = 10.0; Kf = 0.0; $\theta = 0.1$; $D^1 = 3.15 \times 10^{-3}$ m/yr.

A5) Matrix Distribution Coefficient (K_m)

K_m	Z = 10,000 m $\frac{c}{c_0}$	Z = 3,000 m $\frac{c}{c_0}$
0	.950	.985
0.01	.937	.981
0.1	.826	.944
1.0	.240	.652
2.0	.063	.436
5.0	1.4×10^{-3}	.138
10.0	4.1×10^{-6}	2.4×10^{-2}
50.0	6.3×10^{-20}	1.7×10^{-6}
100.0	3.0×10^{-30}	1.4×10^{-9}

$\theta = 0.1$; Kf = 0.0; $b = 1 \times 10^{-4}$; B = 0.4m.; $D^1 = 3.15 \times 10^{-3}$ m/yr.

APPENDIX B

APPENDIX B

Surface Area Available for Adsorption

One way to visualize the apparent inability of the fracture face to adsorb solutes compared to the porous matrix is to compare the surface area available for adsorption.

Fracture Surface Area

Over some cross-sectional area of flow, the total surface area of fractures is dependent on the flow rate because as flow increases the number of fractures increase. For the case of 6500 m^3/yr flowing through a section 1 mile wide, 23 ft (7m) high and 14 miles long the fracture surface area as a function of aperture is given below

2 b(mm)	Area (m^2)
0.1	5.3×10^9
0.2	6.7×10^8
0.4	8.3×10^7
1.0	5.3×10^6
2.0	6.7×10^5

Porous Matrix Area

Serne et al. (1977) estimated the surface area of crushed Magenta and Culebra samples using the ethylene glycol method to be

Magenta	8.1 m^2/g
Culebra	7.1 m^2/g

Assuming a rock density of 2.4×10^6 g/m^3 the surface area is of Culebra would be

$$1.7 \times 10^7 \ \frac{m^2}{m^3}$$

Even if this surface area is a factor of 1000 too large because a crushed sample was used, the surface area of a 40 m^3 block of rock matrix is greater than the entire surface area of fractures 2.0 mm in aperture in a volume 1 mile wide, 14 miles long and 23 feet high (2.5×10^8 m^3).

It is clear that the available surface adsorption sites within the rock matrix are much more numerous than the sites along the fracture face. This is why matrix diffusion and adsorption are so important in retardation of solutes in fracture flow.